IEEE Access
Multidisciplinary | Rapid Review | Open Access Journal

Received January 19, 2020, accepted January 31, 2020, date of publication February 4, 2020, date of current version February 12, 2020.

Digital Object Identifier 10.1109/ACCESS.2020.2971473

Optimization of Torque Ripples in an Interior Permanent Magnet Synchronous Motor Based on the Orthogonal Experimental Method and MIGA and RBF Neural Networks

JINSHUN HAO[1], SHUANGFU SUO[2], YIYONG YANG[1], YANG WANG[1], WENJIE WANG[2], AND XIAOLONG CHEN[1]

[1]School of Engineering and Technology, China University of Geosciences (Beijing), Beijing 100083, China
[2]State Key Laboratory of Tribology, Tsinghua University, Beijing 100084, China

Corresponding author: Shuangfu Suo (sfsuo@mail.tsinghua.edu.cn)

This work was supported by the China Space under Grant 6141B06260405.

ABSTRACT Interior permanent magnet synchronous motors (IPMSMs) have high power densities and speed control performance, and they are widely used in the industry. The problem of reducing the torque ripple of an IPMSM is one of the hot issues in the field of electrical machine design. In order to determine the optimal combination of the geometric parameters to reduce the torque ripple of an IPMSM, a range analysis was conducted on the data from the orthogonal experiments in this study, dividing the rotor geometric parameters into two categories (important and ordinary) based on their degree of impact on the torque ripples of the IPMSM. Thereafter, an optimization of the ordinary parameters was carried out based on the results of the range analysis, whereas the optimization of the important parameters was carried out through a method that combined a multi-island genetic algorithm (MIGA) and Radial Basis Function (RBF) neural networks. The torque ripple of the IPMSM was effectively reduced without materially affecting the output power. Finally, the results of this optimization process were verified using a finite element simulation. The optimization method used in this study divided the motor geometric parameters into two categories and applied a different method of optimization to each parameter type, so it was able to efficiently optimize multiple geometric parameters for the IPMSM.

INDEX TERMS Optimization, permanent magnet machines, genetic algorithms, torque.

I. INTRODUCTION

Interior permanent magnet synchronous motors (IPMSMs) have high power density and speed control performance, and they are widely used in the industry [1]. When an IPMSM is operated, the lower torque ripple levels are conducive to stable torque output, and they reduce the levels of oscillation and the noise of the motor [2]. Hence, low levels of torque ripple are one of the design requisites of IPMSMs. The problem of controlling IPMSM torque ripple is also one of the hot issues in the field of electrical machine design [3].

The reasonable selection of the geometric parameters of an IPMSM can reduce its torque ripple[4]. In order to reduce the torque ripple of IPMSMs, some researchers have tried to optimize their structural parameters. Zhu *et al.* [5] divided the geometric parameters of an IPMSM into two categories based on the importance of the variables to be optimized. Zhu then optimized the geometric parameters of the motors using response surface methodology and the Taguchi method, thus optimizing the motor torque ripples under conditions where the motor output torque remained constant. Lee *et al.* [6] optimized the structural parameters of an IPMSM based on the explorative particle swarm optimization (ePSO) algorithm and finite element analysis software. This optimization reduced the torque ripple. Sorgdrager *et al.* [7] optimized the structure parameters of an IPMSM with the Taguchi method and then achieved a reduction of the torque ripple. Shuhei *et al.* [8] studied IPMSMs and optimized motor

The associate editor coordinating the review of this manuscript and approving it for publication was Mustafa Servet Kiran.

torque ripples by finding the optimal dimensions using a method that combined convolutional neural networks and a genetic algorithm.

In addition, some new structures have reduced the torque ripple of an IPMSM [9]. Ren *et al.* [10] studied inset PMSMs and proposed an asymmetrical V-shaped PMSM structure, adjusting the width ratio and deviation angle from the main axis of the permanent magnets to reduce the cogging torque, thus controlling the PMSM torque ripple. Jiang *et al.* [11] studied the impact of a rotor skew pattern on IPMSM cogging torque and torque ripple and proposed a herringbone rotor skew pattern to suppress motor torque ripples. Kang *et al.* [12] reduced the cogging torque of an IPMSM by putting notches on a rotor pole face, which helped to reduce the torque ripple. Zhou and Chen [13] studied the impact of the shape of a flux-barrier on motor torque ripples and designed three flux-barriers of different shapes to suppress motor torque ripples.

However, when and IPMSM adopts one or more of the above structures to reduce the torque ripple, motor structure will become more complex and the structural parameters related to the motor output performance will become larger, which brings difficulties to the IPMSM topology optimization. For example, when there are many structural parameters to be optimized, the response surface method will become very complicated [14]. An optimization method that combines an algorithm with finite element analysis software takes a long time when there are many structural variables to be optimized [15], [16]. The Taguchi method can achieve the multi-objective optimization of an IPMSM, but it cannot find the optimal combination of parameters, and the optimization result is poor. A neural network needs a large amount of data in the training process, so it takes a lot of time to collect data when the number of structural variables to be optimized is large [17].

In order to reduce the IPMSM torque ripple, the geometric parameters of an IPMSM with two new structures (rotor notch and rotor skew) were optimized in this study. In the first step, the motor geometric parameters were divided into two categories based on a range analysis of the results obtained with the orthogonal experimental method. The first group consisted of ordinary geometric parameters, which had a relatively small effect on the motor torque ripples. The second group consisted of important geometric parameters, which had a greater impact on the motor torque ripples. In the second step, the ordinary geometric parameters were optimized using a range analysis. In the third step, the important geometric variables were optimized using a method that combined a multi-island genetic algorithm (MIGA) and radial basis function (RBF) neural networks. In the final step, the results of the optimization process were verified through a finite element simulation.

Section 2 introduces the optimization process and the motor model optimized in this study. Section 3 describes the optimization of the motor torque ripple. Section 4 describes the verification of the results of the optimization process through finite element simulation. Section 5 summarizes the findings of the study and presents some proposals for future research.

II. OPTIMIZATION PROCESS AND MOTOR MODEL

A. THE OPTIMIZATION PROCESS

The optimization method used to reduce the motor torque ripple in this study is shown in Fig. 1:

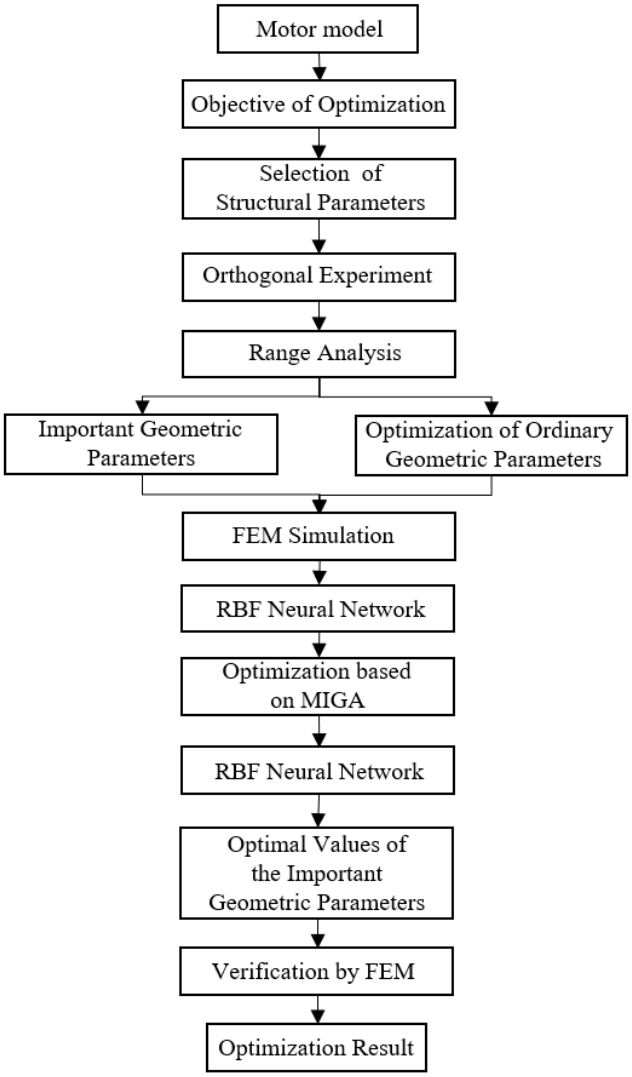

FIGURE 1. Optimization process for the motor.

(1) The structural parameters to be optimized were selected after identifying the objective of optimization.

(2) An orthogonal experimental table was designed based on the number of structural parameters and factor values, and the orthogonal experiment was conducted using a finite element simulation.

(3) A range analysis was performed on the experimental results, and the motor geometric parameters were divided into ordinary geometric parameters and important geometric parameters according to the results thereof.

(4) An indicator-factor graph for the ordinary geometric parameters was plotted based on the results of the range analysis, and the ordinary geometric parameters were optimized based on this graph.

(5) A new model of the motor was constructed based on the outcomes of the optimization.

(6) The impacts of the important geometric parameters on the assessment indicators were obtained through finite element simulation.

(7) An RBF neural network was trained using the data obtained in Step (6).

(8) A MIGA was used to carry out the optimization in the RBF neural network, identifying the optimal values of the important geometric parameters.

(9) The outcomes of this process were then verified using finite element simulation.

B. MOTOR MODEL

As shown in Fig. 2, the optimization of an interior IPMSM was sought in this study. Because a constant outer diameter was one of the dimensional constraints of the stator in the motor used, the optimization of the structural parameters of the rotor was mainly sought in this study. The rotor parameters to be optimized are shown in Fig. 1: magnet thickness H_1, magnet width L_1, magnet web thickness H_2, magnet bridge thickness H_3, pole notch depth H_4, outer arc of pole notch β_1, inner arc of pole notch β_2, pole arc α_1, air gap length L_2, and rotor inner radius R_1. Apart from the ten parameters discussed above, the rotor axial directions of this study were divided into two sections. The mechanical skew angle α_2 between the rotors in each section was also a geometric parameter that needed to be optimized. Hence, in this study a total of eleven geometric parameters of the motor rotor were optimized.

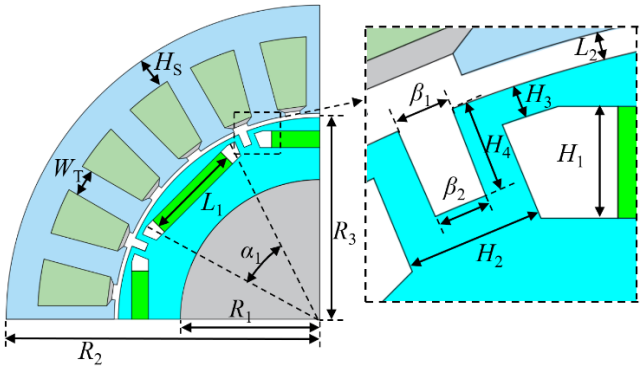

FIGURE 2. Structure diagram of the motor.

The geometric parameters and the winding parameters of the motor that were optimized in this study and are shown in Table 1.

III. OPTIMIZATION OF THE MOTOR TORQUE RIPPLE

A. SIMULATION METHOD

In order to optimize the rotor dimensions, MOTOR-CAD software (version 12.1.7) was used in this study to render

TABLE 1. Parameters of the motor.

Abbreviation	Quantity	Value
H_s (mm)	Thickness of the stator yoke	5
N_s	Slot number	24
Np	Pole number	8
R_1 (mm)	Rotor inner radius	20
R_2 (mm)	Stator outer radius	45
R_3 (mm)	Rotor outer radius	28.9
L_m	Stack length (mm)	50
W_T (mm)	Tooth width	3.85
H_1 (mm)	Magnet thickness	2.4
L_1 (mm)	Magnet width	13.8
H_2 (mm)	Magnet web thickness	3
H_3 (mm)	Magnet bridge thickness	0.7
H_4 (mm)	Pole notch depth	2
β_1 (mm)	Outer arc of pole notch	10
β_2 (mm)	Inner arc of pole notch	10
α_1 (°)	Pole arc	135
L_2 (mm)	Air gap length	0.6
α_2 (°)	Mechanical skew angle	1.2
P	Pitch	3
N_L	Winding layer	1
N_T	Turns	26

simulations of the motor. All of the simulated data were derived using this software. During the simulation process, the motor mesh subdivision used is shown in Fig. 3. The air gap (where the changes in the magnetic field were the most complicated) was divided into four layers to obtain more precise calculations. During the simulation process, only the geometric parameters of the motor rotor were changed.

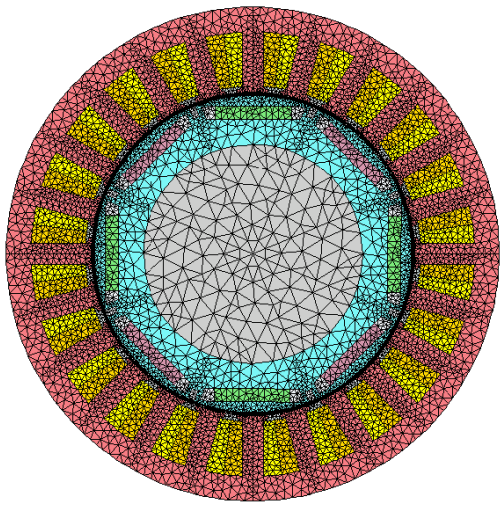

FIGURE 3. The mesh of the motor model.

B. CLASSIFICATION OF THE MOTOR PARAMETERS AND THE INITIAL OPTIMIZATION

The orthogonal experimental method is a scientific method that uses the principles of statistics and orthogonality to select from a large set of design points those are appropriate and representative in order to rationally design an experiment. This method has the advantages of being able to substantially reduce the number of experiments, thus reducing the amount of labor involved [18]. For instance, the eleven factors (with three different values for each) evaluated in this

TABLE 2. Range analysis results.

Geometric Parameters	Range analysis result	Geometric Parameters	Range analysis result
H_1 (mm)	0.1922	β_2 (mm)	0.1044
L_1 (mm)	0.1611	α_1 (°)	0.5800
H_2 (mm)	0.1700	L_2 (mm)	0.2556
H_3 (mm)	0.2100	R_1 (mm)	0.1356
H_4 (mm)	0.0644	α_2 (°)	0.6222
β_1 (mm)	0.2144		

study would normally require $3^{11} = 177,147$ experiments. If the experiment was carried out according to the L27(3^{11}) orthogonal array, then only 27 experiments would need to be conducted. Additionally, because the experiment points were uniformly distributed throughout the optimal selection range, the orthogonal experimental method could ensure that no possible factor combinations were left out.

Range analysis is one way to analyze the results obtained with the orthogonal experimental method. The method allows for the ordering of the degree of impact by each factor based on assessment indicators as well as the optimization of these factors. See reference [19] for a detailed introduction to range analysis.

There were eleven factors considered in the orthogonal experiments conducted for this study (the eleven geometric parameters listed in Section 2), and three values were considered for each factor. See reference [19] for more details on the orthogonal experimental method.

The results of the range analysis on the results obtained with the orthogonal experimental results are shown in Table 2. The impact of the motor structural parameters on the torque ripples could be ranked from largest to smallest:

$\alpha_2 > \alpha_1 > L_2 > \beta_1 > H_3 > H_1 > H_2 > L_1 > R_1 > \beta_2 > H_4$.

The motor rotor structural parameters could be divided into two categories based on the results of the range analysis:

Ordinary geometric parameters: H_1, H_2, L_1, R_1, β_2, H_4. Important geometric parameters: α_2, α_1, L_2, β_1, H_3.

Fig. 4 shows the indicator-factor graphs for the ordinary geometric parameters and the torque ripple obtained through the range analysis: the torque ripple first rises and then declines with the increase of H_4, the torque ripple first declines and then rises with the increase of β_2 and H_2, the torque ripple rises gradually with the increase of R_1, the torque ripple declines gradually with the increase of H_1 and L_1. As discussed in Section 3.1, the ordinary geometric parameters were optimized based on those range analysis results. The optimization results are shown in Table 3.

TABLE 3. Optimized ordinary geometric parameters.

Geometric Parameters	Original value	After optimization
H_4 (mm)	2	3
β_2 (mm)	10	10
H_1 (mm)	2.4	2.8
L_1 (mm)	13.8	14.3
H_2 (mm)	3	3
R_1 (mm)	20	18

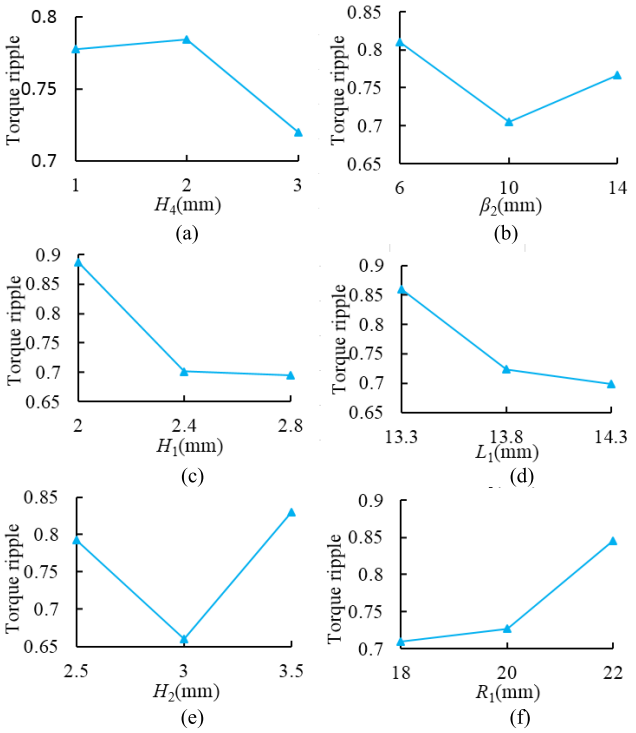

FIGURE 4. Indicator-factor graph for the ordinary geometric parameters. (a) Effect of H_4 on torque ripple. (b) Effect of β_2 on torque ripple. (c) Effect of H_1 on torque ripple. (d) Effect of L_1 on torque ripple. (e) Effect of H_2 on torque ripple. (f) Effect of R_1 on torque ripple.

C. OPTIMIZATION OF THE IMPORTANT MOTOR GEOMETRIC PARAMETERS BASED ON THE RBF NEURAL NETWORKS AND THE MIGA

As discussed in Section 3.1, the important geometric parameters (the second category) were optimized using a method that applied a MIGA to the RBF neural networks. The RBF neural networks had the universal approximation ability, and they did not suffer from the problem of a local minimum [20]. As shown in Fig. 5, the RBF neural networks were divided into three layers—an input layer, a hidden layer, and an output layer, where the output layer was the response to the input. The output layer in an RBF neural network employs linear optimization strategies, which allows for faster learning. In this study, an RBF neural network was trained to predict the torque tipple of IPMSMs. See reference [21] for a detailed introduction to RBF neural networks.

In this study, 6300 groups of simulation data (from MOTOR-CAD software) were used to train the RBF neural network. The dataset obtained from the finite element simulation can be described as

$$\begin{cases} E = f(\beta_1, H_3, \alpha_2, L_2, \alpha_3) \\ 6\text{mm} \le \beta_1 \le 14\text{mm}, \textit{step}{:}2\text{mm} \\ 0.5\text{mm} \le H_3 \le 0.9\text{mm}, \textit{step} : 0.1\text{mm} \\ 120^\circ \le \alpha_1 \le 150^\circ, \textit{step} : 5\text{mm} \\ 0.4\text{mm} \le L_2 \le 0.8\text{mm}, \textit{step} : 0.1\text{mm} \\ 0\text{mm} \le \alpha_2 \le 2.4\text{mm}, \textit{step} : 0.3\text{mm} \end{cases} \quad (1)$$

Multi-island genetic algorithm (MIGA) is a kind of parallel genetic algorithm based on a traditional genetic algorithm.

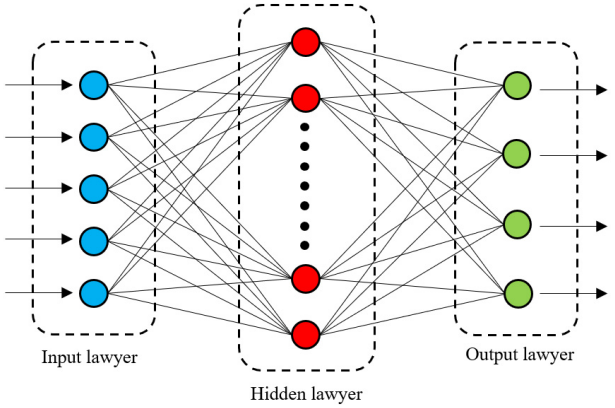

FIGURE 5. RBF neural network.

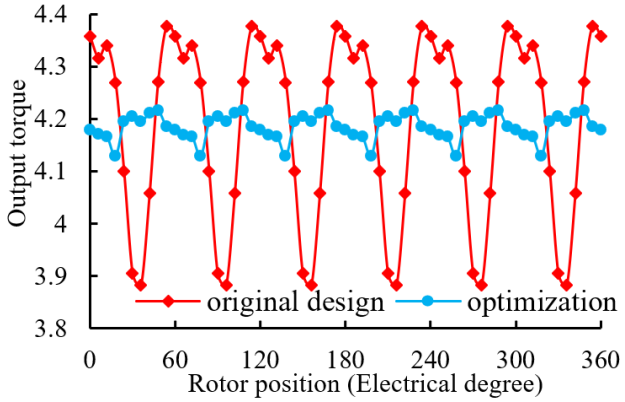

FIGURE 6. Optimization result of the torque ripple.

However, in comparison to a traditional genetic algorithm, a MIGA divides an entire population into many sub-populations that are mutually separated, thus isolating them on different "islands." Traditional genetic algorithm operations are then performed on the individuals in every sub-population so that the entire population becomes more diversified. Thus, the incidence of a precocious phenomenon in the optimization process is suppressed [22]. Such improvements allow a MIGA to solve global optimal solutions better and to have higher computation efficiency. In this study, a MIGA was used to optimize the RBF neural networks and then identify the optimal values of the important geometric parameters. The optimization process can be described as follows:

$$\begin{cases} E = \min f(\beta_1, H_3, \alpha_2, L_2, \alpha_3) \\ 6\text{mm} \le \beta_1 \le 14\text{mm} \\ 0.5\text{mm} \le H_3 \le 0.9\text{mm} \\ 120^\circ \le \alpha_1 \le 150^\circ \\ 0.4\text{mm} \le L_2 \le 0.8\text{mm} \\ 0\text{mm} \le \alpha_2 \le 2.4\text{mm} \\ P_{out} \ge 5000\text{W} \end{cases} \quad (2)$$

The optimization results are as shown in Table 4. Post-optimization, the torque ripple was reduced by 83.2%, from 0.482 Nm to 0.081 Nm, while the output power remained fundamentally unchanged.

TABLE 4. Optimized important geometric parameters.

Parameters	Original Value	After Optimization
H_3 (mm)	0.70	0.71
β_1 (mm)	10	7.5
α_1 (°)	150	149
L_2 (mm)	0.60	0.55
α_2 (°)	1.20	1.85
E (mm)	0.482	0.081
P_{out}	5019 W	5001 W

IV. VERIFICATION OF THE OPTIMIZATION RESULTS

In order to verify the accuracy of the optimization results, calculations were performed on the post-optimization motor torque ripples using finite element selection. As shown

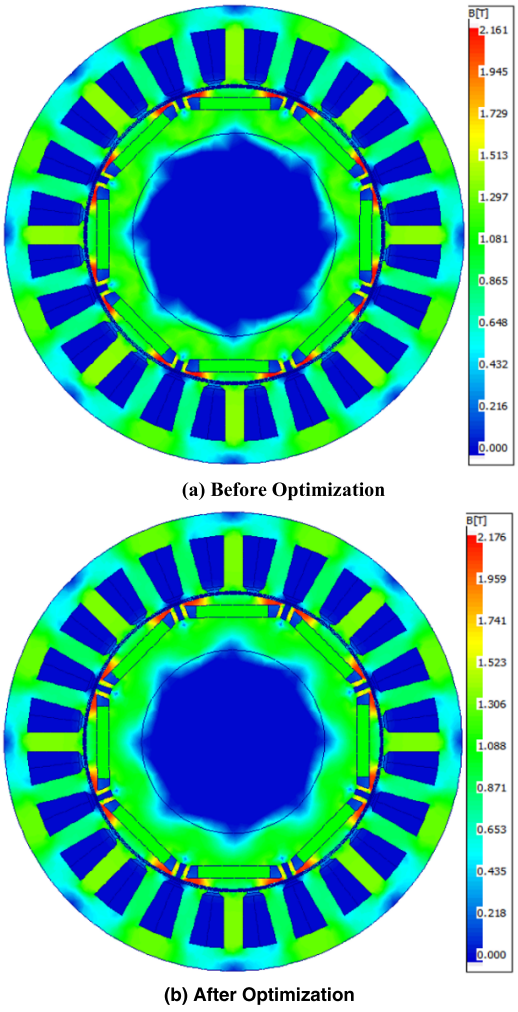

FIGURE 7. Flux distribution.

in Fig. 6, the results showed that the post-optimization motor torque ripples were 84% lower at 0.077 Nm (an error of 4.9% compared to the optimized values), compared to 0.482 Nm in the initial design. Furthermore, the results of the simulation showed that the post-optimization motor output power was 5010 W, compared to a pre-optimization level of 5019 W,

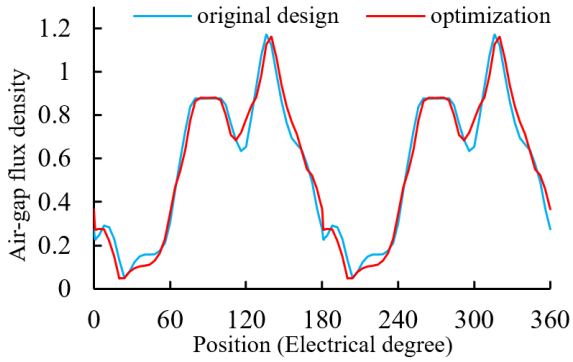

FIGURE 8. Air-Gap flux density.

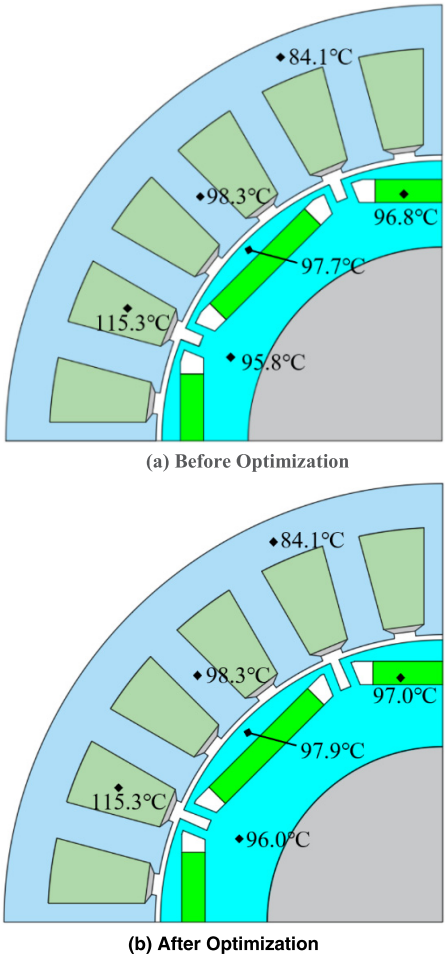

FIGURE 9. Steady-state temperature of the IPMSM.

meaning that the post-optimization output power remained fundamentally unchanged.

Fig. 7 shows the magnetic field distributions of the two motors. As shown in Fig. 7, except for the fact that the flux saturation at the magnetic bridge was more serious, the magnetic field distribution of the optimized IPMSM was essentially unchanged.

Fig. 8 shows the air-gap flux density of the two motors. As shown in Fig. 8, the peak air gap magnetic density of the IPMSM before and after optimization was close to 1.2 t,

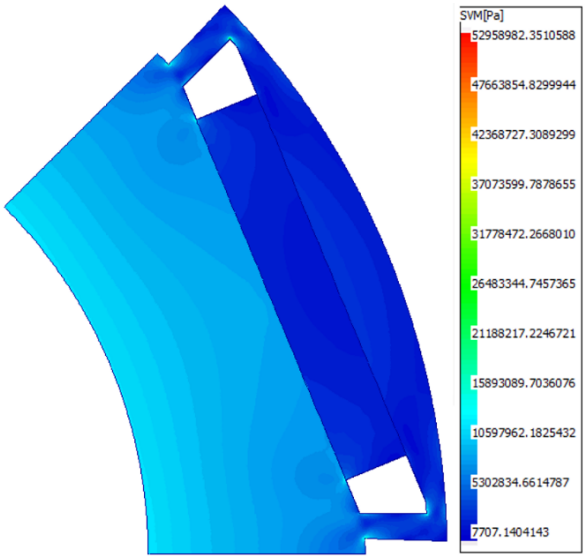

FIGURE 10. Von mises stress of the rotor.

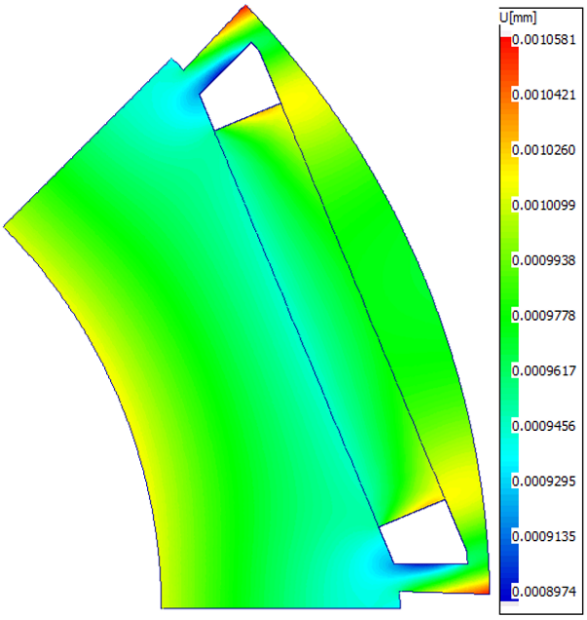

FIGURE 11. Distortion of the rotor.

which meant that the permanent magnet material (n42uh) could be fully utilized.

Motor CAD software was used to calculate the steady-state temperature of the IPMSM based on the thermal-circuit method. The calculation results showed that the internal temperature field distribution of the IPMSM before and after optimization was essentially unchanged (as shown in Fig. 9). In addition, the maximum temperature of the optimized motor was 115.3°C, which was lower than the operating temperature limit (150°C) and which had enough of a stability margin to meet the long-term operation conditions.

To verify the mechanical reliability of the optimized IPMSM (as shown in Fig. 10), the mechanical stress of its rotor was calculated using FEM. The von Mises stress was

53 MPa, which was much smaller than the yield strength (305 MPa), so the rotor was safe and reliable. The calculation results also showed that the maximum distortion of the rotor (as shown in Fig. 11) was 0.0011 mm.

V. CONCLUSION

In this study, torque ripples were optimized in inset PMSMs using a MIGA, RBF neural networks, and the orthogonal experimental method. First, motor geometric parameters were used as factors, and torque ripples were used as assessment indicators in the orthogonal experiments. In the second step, a range analysis was conducted on the results obtained with the orthogonal experimental method. The results were used to classify the geometric parameters as ordinary or important. In the third step, the ordinary geometric parameters were optimized using the results of the range analysis. Finally, the important geometric parameters were optimized using a method that combined RBF neural networks and a MIGA. Some key conclusions are summarized as follows:

a) It was verified (through finite element analysis) that the torque ripples of the IPMSM are reduced by 84% after optimization. The optimization results indicated that the method used in this study could effectively optimize and minimize the torque ripple of the IPMSM.
b) The error between the optimization results and the finite element analysis results was 4.9%. The comparison results showed that the optimization method used in this study could accurately predict the optimization results of the torque ripple.
c) In this study, eleven structural parameters are successfully optimized to minimize the torque ripple of the IPMSM. The optimization result showed that the optimization method used in this study could effectively optimize the multi structural parameters of the IPMSM.

In addition, researchers can use this method when optimizing structural parameters to improve other motor attributes (such as power density, losses, and noise).

However, if there were many important geometric parameters to be optimized, the optimization method used in this study would still require large amounts of simulation data to train the RBF neural networks, which will be a highly time-consuming step. In the future, the author intends to work on a solution to this problem.

REFERENCES

[1] J. Yang, W.-H. Chen, S. Li, L. Guo, and Y. Yan, "Disturbance/uncertainty estimation and attenuation techniques in PMSM drives—A survey," *IEEE Trans. Ind. Electron.*, vol. 64, no. 4, pp. 3273–3285, Apr. 2017.
[2] M. Li and W. Wang, "Influence of salient-pole torque on torque ripple of interior permanent magnet synchronous motor," *Micromotors*, vol. 51, no. 2, pp. 11–14, 2018.
[3] Q. Liu and K. Hameyer, "Torque ripple minimization for direct torque control of PMSM with modified FCSMPC," *IEEE Trans. Ind. Appl.*, vol. 52, no. 6, pp. 4855–4864, Nov. 2016.
[4] X. Liu, H. Chen, J. Zhao, and A. Belahcen, "Research on the performances and parameters of interior PMSM used for electric vehicles," *IEEE Trans. Ind. Electron.*, vol. 63, no. 6, pp. 3533–3545, Jun. 2016.
[5] X. Zhu, W. Wu, L. Quan, Z. Xiang, and W. Gu, "Design and multi-objective stratified optimization of a less-rare-earth hybrid permanent magnets motor with high torque density and low cost," *IEEE Trans. Energy Convers.*, vol. 34, no. 3, pp. 1178–1189, Sep. 2019.
[6] J. H. Lee, J.-W. Kim, J.-Y. Song, Y.-J. Kim, and S.-Y. Jung, "A novel memetic algorithm using modified particle swarm optimization and mesh adaptive direct search for PMSM design," *IEEE Trans. Magn.*, vol. 52, no. 3, Mar. 2016, Art. no. 7001604.
[7] A. J. Sorgdrager, R.-J. Wang, and A. J. Grobler, "Robust torque ripple mitigation of a line-start PMSM by means of the taguchi method," in *Proc. SAUPEC/RobMech/PRASA*, Bloemfontein, South Africa, Jan. 2019, pp. 1–6.
[8] S. Doi, H. Sasaki, and H. Igarashi, "Multi-objective topology optimization of rotating machines using deep learning," *IEEE Trans. Magn.*, vol. 55, no. 6, Jun. 2019, Art. no. 7202605.
[9] Y. Hu, Y. Xiao, B. Chen, and Q. Li, "Topology optimization of a consequent-pole rotor with V-shaped magnet placement," in *Proc. 21st ICEMS*, Jeju, South Korea, Oct. 2018, pp. 234–239.
[10] W. Ren, Q. Xu, Q. Li, and L. Zhou, "Reduction of cogging torque and torque ripple in interior PM machines with asymmetrical V-type rotor design," *IEEE Trans. Magn.*, vol. 52, no. 7, Jul. 2016, Art. no. 8104105.
[11] J. W. Jiang, A. Emadi, H. Dadkhah, Y. Yang, A. Sathyan, and B. Bilgin, "Rotor skew pattern design and optimisation for cogging torque reduction," *IET Electr. Syst. Transp.*, vol. 6, no. 2, pp. 126–135, Jun. 2016.
[12] G.-H. Kang, Y.-D. Son, G.-T. Kim, and J. Hur, "A novel cogging torque reduction method for interior-type permanent-magnet motor," *IEEE Trans. Ind. Appl.*, vol. 45, no. 1, pp. 161–167, Jan./Feb. 2009.
[13] T. Zhou and J.-X. Shen, "Cogging torque and operation torque ripple reduction of interior permanent magnet synchronous machines by using asymmetric flux-barriers," in *Proc. 20th Int. Conf. Electr. Mach. Syst. (ICEMS)*, Sydney, NSW, Australia, Aug. 2017, pp. 1–6.
[14] G. Lei, J. Zhu, Y. Guo, C. Liu, and B. Ma, "A review of design optimization methods for electrical machines," *Energies*, vol. 10, no. 12, p. 1962, Nov. 2017.
[15] T. Song, Z. Zhang, H. Liu, and W. Hu, "Multi-objective optimisation design and performance comparison of permanent magnet synchronous motor for EVs based on FEA," *IET Electr. Power Appl.*, vol. 13, no. 8, pp. 1157–1166, Aug. 2019.
[16] S. Shimokawa, H. Oshima, K. Shimizu, Y. Uehara, J. Fujisaki, and A. Furuya, "Fast 3-D optimization of magnetic cores for loss and volume reduction," *IEEE Trans. Magn.*, vol. 54, no. 11, Nov. 2018, Art. no. 8400904.
[17] H. Sasaki and H. Igarashi, "Topology optimization of IPM motor with aid of deep learning," *Int. J. Appl. Electromagn. Mech.*, vol. 59, no. 1, pp. 87–96, Mar. 2019.
[18] Y. Zhu, W. Wei, C. Yang, and Y. Zhang, "Multi-objective optimisation design of two-phase excitation switched reluctance motor for electric vehicles," *IET Electr. Power Appl.*, vol. 12, no. 7, pp. 929–937, Aug. 2018.
[19] W. He and B. Tang, *Optimizing Experiments Design Method and Data Analysis*, vol. 2, 1st ed. Beijing, China Chemical Industry Press, 2012, pp. 1–59.
[20] S. Bakire, X. Yang, G. Ma, X. Wei, H. Yu, J. Chen, and H. Lin, "Developing predictive models for toxicity of organic chemicals to green algae based on mode of action," *Chemosphere*, vol. 190, pp. 463–470, Jan. 2018.
[21] F. Gao, *MATLAB Intelligent Algorithm Learning Manual*, 1st ed. Beijing, China: Posts & Telecom Press, 2014, pp. 135–157.
[22] N. Ma, H. Lei, Z. Han, D. Zhou, Y. Bao, K. Zhang, L. Zhou, and C. Chen, "Airfoil optimization to improve power performance of a high-solidity vertical axis wind turbine at a moderate tip speed ratio," *Energy*, vol. 150, pp. 236–252, May 2018.

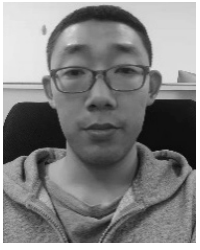

JINSHUN HAO was born in Baoding, Hebei, China, in 1995. He received the B.S. degree in mechanical engineering from the China University of Geosciences, Beijing, where he is currently pursuing the M.S. degree.

His research interests include high-performance permanent magnet synchronous motor and multiobjective optimization method of motor.

SHUANGFU SUO was born in Tangshan, Hebei, China. He received the B.S., M.S., and Ph.D. degrees in mechanical engineering from the China University of Mining and Technology.

From April 1996 to April 1998, he was a Postdoctoral Student with the Research Group of Prof. L. Jiajun, Department of Mechanical Engineering, Tsinghua University. From May 1985 to September 1988, he was engaged in the research of elevator with the China University of Mining and Technology, where he was engaged in scientific research and teaching, from February 1991 to September 1992. Since May 1998, he has been engaged in the research and basic research of mechatronics equipment with the Department of Precision Instruments and Mechanics, Institute of Mechanical Design, Tsinghua University. Since he took part in the work, he has published more than 70 articles and obtained 26 patents. His main research areas are mechatronics and high-performance permanent magnet synchronous motor design.

YIYONG YANG received the Ph.D. degree in mechanical engineering from Tsinghua University.

Since 2004, he has been engaged in mechanical engineering, vehicle engineering, and other related scientific research with the China University of Geosciences. His current research interest includes high-power density motor design and its' cooling methods.

YANG WANG was born in Liaoning, China. He received the B.S. degree in mechanical engineering from the China University of Geosciences, Beijing, where he is currently pursuing the Ph.D. degree.

His research interests include high-performance permanent magnet synchronous motor design and fuzzy singular perturbation control.

WENJIE WANG was born in Shanxi, China, in 1995. He received the B.S. degree in mechanical engineering from Chongqing University, Chongqing. He is currently pursuing the M.S. degree with Tsinghua University.

His research interest includes high-performance permanent magnet synchronous motor and its' cooling method.

XIAOLONG CHEN was born in Shandong, China. He received the B.S. degree in mechanical engineering from Shandong Jianzhu University, Jinnan. He is currently pursuing the M.S. degree with the China University of Geosciences, Beijing.

His research interest includes high-speed bearing design and its' multiobjective optimization methods.